Biochemical and Biophysical Research Communications 632 (2022) 100–106

Contents lists available at ScienceDirect

Biochemical and Biophysical Research Communications

journal homepage: www.elsevier.com/locate/ybbrc

Dose-enhancement of MCF 7 cell line radiotherapy using silica-iron oxide nanocomposite

Mohamed M. Fathy [a], Omnia A. Saad [a, *], Wael M. Elshemey [b], Heba M. Fahmy [a]

[a] Biophysics Department, Faculty of Science, Cairo University, 12613, Giza, Egypt
[b] Department of Physics, Faculty of Science, Islamic University in Madinah, Saudi Arabia

ARTICLE INFO

Article history:
Received 8 September 2022
Received in revised form
10 September 2022
Accepted 22 September 2022
Available online 27 September 2022

Keywords:
Iron oxide magnetic nanoparticles (IONPs)
Radiation therapy
Nano-radiosensitizer
Breast cancer
Cytotoxicity

ABSTRACT

Cancer radiotherapy is one of the most effective regimens of cancer treatments, but cancer cell radioresistance remains a concern. Radiosensitizers can selectively improve the efficacy of radiotherapy and reduce inherent damage. The purpose of this work is to evaluate the effect of silica-coated iron oxide magnetic nanoparticles (SIONPs) as a radiosensitizer and compare their therapeutic effect with that of Iron oxide magnetic nanoparticles (IONPs). IONPs and SIONPs were characterized using several physical techniques such as a transmission electron microscope (TEM) and Vibrating sample magnetometer (VSM). MTT and DNA double-strand breaks (Comet) assays have been used to detect the cytotoxicity, cell viability, and DNA damage of MCF-7 cells, which were treated with different concentrations of prepared nanoparticles and exposed to an X-ray beam. In this study, an efficient radiosensitizer, SIONPs, was successfully prepared and characterized. With 0.5 Gy dose, dose enhancement factor (DEF) values of cells treated with 5 and 10 μg/ml of IONPs were 1 and 1.09, respectively, while those treated with SIONPs at these concentrations had DEF of 1.21 and 1.32, respectively. Results demonstrated that SIONPs provide a potential for improving the radiosensitivity of breast cancer.

1. Introduction

Radiotherapy (RT), a noninvasive treatment strategy, was commonly used for malignant cancers as primary treatment [1,2]. Cancer radioresistance is considered an important obstacle was limiting the use of RT with hypoxic tumors [3–7].

Reactive oxygen species (ROS) generation is vital for inducing the indirect effects of RT due to its interaction with biomolecules. DNA damage, protein oxidation, or lipid peroxidation are all possible scenarios resulting from this interaction, triggering apoptosis [8]. Research has indicated that radiation sensitizers can improve the anticancer output of RT by overcoming the disadvantages of radiation. Recently, designing and developing radiosensitizers that can enhance RT's anti-carcinogenic performance via the stimulation of ROS production is considered a good and successful strategy for effective cancer treatment [9,10].

Because of their wide applications in biological and medical sciences, nanoparticles have acquired great attention [11,12]. Nanoparticles are important in nanodiagnostics and cancer radiation treatment. They are currently commonly employed to deliver medications to precise spots in a regulated way, including whole organs and single cells [13]. Recently the clinical results of radiation therapy were improved with the use of nano-radiosensitizers [14,15] because of their ability to improve radiation effectiveness in cancerous cells by improving the generation of ROS [16].

Because of super-para-magnetism, which enables iron oxide magnetic nanoparticles (IONPs) to be influenced by external magnetic field exposure [17] and biocompatibility, IONPs had been qualified to be used as theragnostic agents [18,19].

One of the barriers to using magnetic nanoparticles in medical applications is the van der Waals force and the magnetic attraction between particles because of the high surface energy, which causes agglomeration [20]. The coating process of IONPs can overcome this obstacle by using a biocompatible material that converts IONPs to hydrophilic, bio-compliant, effective, and stable nanoparticles [21–23].

Silica is known to be among the most appropriate IONPs coats [24–26]as it improves the stability of IONPS without influencing its magnetic properties [27]. The internal magnetic core of iron oxide supplies magnetic properties of nanoparticles, while chemical

* Corresponding author.
E-mail address: oashraf@sci.cu.edu.eg (O.A. Saad).

https://doi.org/10.1016/j.bbrc.2022.09.087
0006-291X/

stability and biological compatibility are provided via silica shell [26,28]. Silica nanoparticles have been used as radiosensitizing agents because they improve mitochondrial ROS generation [29]. This means using silica nanoparticles as an IONPs coat can enhance its radiation effect.

A previous study indicated that the silica coating layer improved the radiosensitizing effect of IONPs when combined with electron therapy [27].

According to the author, this is the first research that includes a study of the radiotherapeutic impact of iron oxide nanoparticles coated with silica (SIONPs) on the radiological sensitivity of cancer cells when combined with megavoltage energy X-ray. This study aims to prepare SIONPs and examine their radioenhnacing effect on cancerous cells during X-ray photon therapy.

2. Materials and methods

2.1. Materials

Chemicals for IONPs and SIONPs preparation, Ferric chloride ($FeCl_3.6H_2O$), Ferrous chloride ($FeCl_2$. $4H_2O$), 28% w/v % ammonia hydroxide solution, Tetraethyl orthosilicate (TEOS), were ordered from Sigma-Aldrich (Germany).

For MTT and comet assays, Trypsin, 70% (v/v) ethanol,10% fetal bovine serum (FBS), L-glutamine), Tris-borate- EDTA (TBE), penicillin, streptomycin,3-(4,5-dimethylthiazol-2-yl) 2,5diphenyl tetrazolium bromide (MTT), EtBrstain, Phosphate buffered saline (PBS), RPMI-1640 medium, and dimethyl sulphoxide (DMSO) werebought through Sigma-Aldrich (Germany).

The human epithelial breast cancer cell line (MCF-7 RRID: CVCL_0031) was obtained from the American type culture collection; in Manassas, VA, USA (ATCC®: HTB-22™) via the biological Commodity and Vaccines holding firm (Vacsera, Cairo, Egypt).

2.2. Methods

2.2.1. Synthesis of IONPs nanoparticles

The co-precipitation protocol by Elbialy et al. has been applied to prepare IONPs with some modifications [30]. By mechanical stirring, 80 mL of deionized water was used to dissolve $FeCl_2 \cdot 4H_2O$ and $FeCl_3 \cdot 6H_2O$ (1: 2 mg/ml). The reaction was kept at 80 °C for 30 min with a dropwise addition of 10 ml ammonia solution (28 wt%).

2.2.2. Synthesis of SIONPs nanoparticles

The coating process was carried out using the method described by Fathy et al. [27]. Briefly, 30 ml of ethanol was added to 120 ml of deionized water and 100 mg of IONPs. For dispersion, the mixture was kept in an ultrasonicator for 15 min, then 28 wt % ammonia hydroxide solution and TEOS were drop wisely added (4.6 ml and 2 ml, respectively). The reaction was magnetically stirred at room temperature for 24h. The brown product was dried at 80 °C for 10 h after being rinsed with ethanol and then deionized water many times.

2.2.3. Physical characteristics of the IONPs and SIONPs

The morphology of IONPs and SIONPs was observed by a transmission electron microscope (TEM) (JEM 1230 electron microscope. Jeol, Tokyo, Japan).

Dynamic light scattering (DLS) was used for the size distribution measurements of suspended nanoparticles. The size was measured as a hydrodynamic diameter (NP core + surface-binding solvent layer) using Zeta Potential/Particle Sizer (NICOMP TM 380 ZLS, USA), which investigates the size distribution and zeta potential of IONPs and SIONPs.

The atomic force microscope (AFM) (Wet − SPM9600. Japan) investigated surface topography, shape, and roughness.

The magnetic properties of IONPs and SIONPs were determined using the vibrating sample magnetometer (VSM). The superparamagnetic behavior of IONPs and SIONPs was investigated using VSM (LakeShore 7410, LakeShore, and Westerville, USA).

2.2.4. Irradiation setup

At 37 °C, RPMI-1640 medium supplemented with 10% FBS, L-glutamine, penicillin, and streptomycin was used as a growing medium for MCF-7 cells and brooded in a CO_2 incubator. 6 MeV X-ray photon beam (precise, Electa, Sweden) was adjusted to irradiate culture plates with 14 × 14 cm^2 field size and 100 cm source-to-cell surface distance [27].

2.2.5. Cell viability assay

In 96 well plates, MCF-7 cells (10^4 cells/well) were cultivated and kept for 48 h to attach. Subsequently, the incubation of MCF 7 cells with IONPs and SIONPs at 37 °C with different concentrations (0, 5, 10, 20, 40, and 80 μg/ml). 24hr after incubation, cells were irradiated with 0, 0.5, 1, 2, and 4 Gy. The percentage of cell viability was measured 24hr after irradiation by MTT assay after staining the treated cells with 0.5 MTT stain (25 μl/well) for 2 h. In 0.05 ml of DMSO, the formed MTT formazan crystals were dissolved on a plate shaker for 30 min. An ELISA plate reader (Biotek 8000; USA) was used to measure Optical densities (OD) at 570 nm. Cell viability % was calculated by dividing the OD of treated cells by that of untreated cells [31].

Dose enhancement factor (DEF) values were calculated by using the following equation:

$$DEF = \frac{\text{viability of the cells treated with radiation dose only}}{\text{viability of cells treated with combined therapy (prepared NPs + radiation dose)}} \quad [16]$$

2.2.6. Comet assay

The comet assay measured the three major parameters, tail length, % DNA in the tail, and the tail moment. These parameters reflect the DNA damage caused by IONPs and SIONPs.

In two (6 well) plates, MCF-7 cells were cultivated, then IONPs, SIONPs, and SIONPs were added at 10 and 40 μg/ml concentrations. 24hr after treatment, each plate was divided into five groups; as illustrated in Table 1, one plate was irradiated with 0.5 Gy, and the other plate was irradiated with 1 Gy. 24 hr after irradiation, cells were re-suspended in 100 μL of PBS after being washed with trypsin.

The cell suspension was added to melted LM agarose, and 75 μL of this mixture was fully distributed on the sample area of a pre-warmed comet slide. Then the slide was kept for 10 min at 4 °C for solidification. For 40 min in the dark, slides were immersed in an alkaline medium and then washed with Tris-Borate-EDTA (TBE). For 20 min, the electrophoresis process was applied over the slides and kept overnight for air drying.

From 100 cells/sample, averages of comet parameters (the tail

Table 1
MCF-7 cells groups that treated with IONPs and SIONPs at (10 and 40 μg/ml) and exposed to x-ray radiation with doses of 0.5 and 1 Gy.

Groups	Treatment regimen
0.5G1	cells exposed to radiation only (0.5 Gy)
0.5G2	cells were treated with 10 μg/ml of IONPs + exposed to radiation (0.5 Gy)
0.5G3	cells were treated with 10 μg/ml of SIONPs + exposed to radiation (0.5 Gy)
0.5G4	cells were treated with 40 μg/ml of IONPs + exposed to radiation (0.5 Gy)
0.5G5	cells were treated with 40 μg/ml of SIONPs + exposed to radiation (0.5 Gy)
1G1	cells exposed to radiation only (1 Gy)
1G2	cells were treated with 10 μg/ml of IONPs + exposed to radiation (1 Gy)
1G3	cells were treated with 10 μg/ml of SIONPs + exposed to radiation (1 Gy)
1G4	cells were treated with 40 μg/ml of IONPs + exposed to radiation (1 Gy)
1G5	cells were treated with 40 μg/ml of SIONPs + exposed to radiation (1 Gy)

length, % DNA in tail and tail moment) were measured using the software program, comet score, version 5.0.

2.2.7. Statistical analysis

At least three separate experiments were carried out, and results were specifically collected as average ± SD.

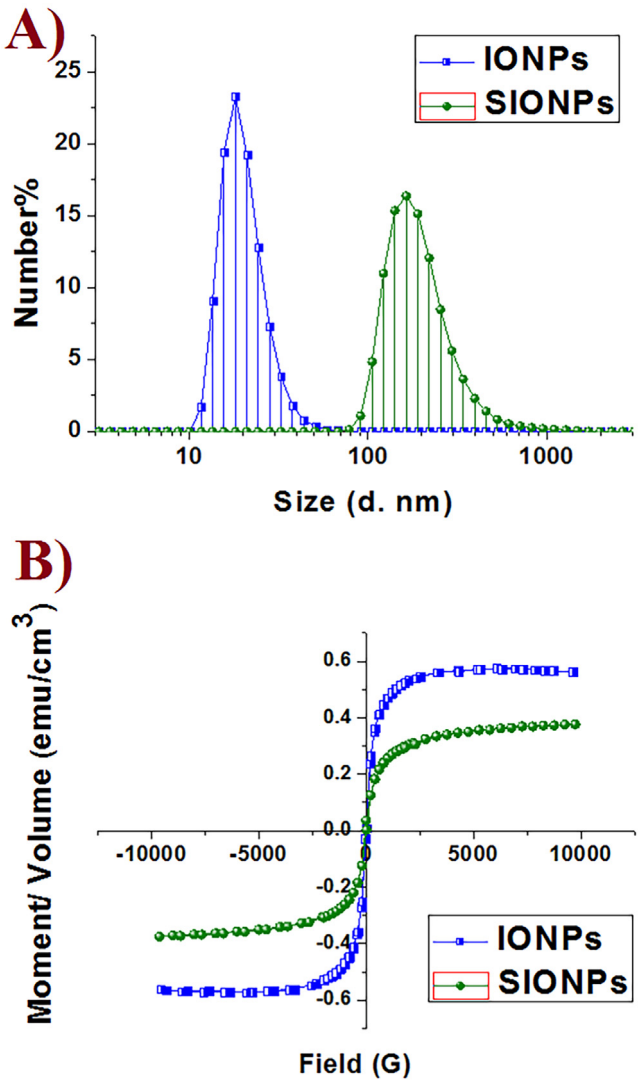

Fig. 1. (A) Particle size distribution of IONPs and SIONPs, (B) Magnetization curves of IONPs and SIONPs.

For the comet test, SPSS was used to conduct a one-way Variance Analysis (ANOVA). With $P < 0.05$, Scheffe's test was conducted for independent and dependent groups as a post-hoc comparison.

3. Results and discussion

3.1. Physical characteristics of IONPs and SIONPs

3.1.1. Size distribution

The average particle size of IONPs and SIONPs, analyzed from the dynamic light scattering (DLS) results, was 18.17 ± 4.5 nm and 164.18 ± 16.1 nm, respectively (Fig. 1A). Since the DLS technique measures the diameter of particles in aqueous environments, including hydration shells, this diameter is known as a hydrodynamic diameter [32]. The measurements can be impacted by particle agglomeration [33]and hydrodynamic conditions [34]. The polydispersity index (PDI) values of IONPs and SIONPs gave the impression that IONPs have homogenous size distribution while SIONPs have a slight broadening in their size distribution [35].

3.1.2. Morphological study

Morphological information of the prepared nanoparticles was obtained using transmission electron microscopy (TEM) and Atomic force microscopy (AFM). TEM image of IONPs (Fig. 2A) represents the spherical shape structure with an average diameter of 13.63 ± 1.36 nm. In the core-shell structure of SIONPs demonstrated in Fig. 2B, the silica coat has been formed into a multi-layered pattern with a thickness of about 43.35 ± 2 nm, and the average core diameter was about 54.9 ± 10.1 nm.

The core-shell structure, multi-layered coverage, and thickness uniformity of silica coat are well demonstrated in the SIONPs TEM image. This proves that the silica layer can preclude IONPs aggregation. Yin et al. demonstrated that the thickness of the silica coat could be affected by changing the TEOS solution concentration and/or the reaction time [36].

Using AFM, topographic information, particle size, and surface roughness of IONPs and SIONPs were investigated. In Fig. 2C and D illustrated that there were several small cavities with a uniform distribution pattern on the IONPs surface (Fig. 2C), while SIONPs have a granular surface (Fig. 2D).

From AFM data analysis, the particle size of IONPs and SIONPs was 15.6 ± 3.5 nm and 152.3 ± 8.9 nm, respectively. These results correlate well with the TEM results.

Surface roughness results were found to be1.878 ± 0.03 and 2.489 ± 0.12 nm for IONPs and SIONPs, respectively. Surface roughness controls the intensity of nanoparticle-cell reactions, improves cell absorption, and supports cell adhesion [37–39]. Surface roughness changes may change the contact potential between absorbing molecules and the nanoparticle [40].

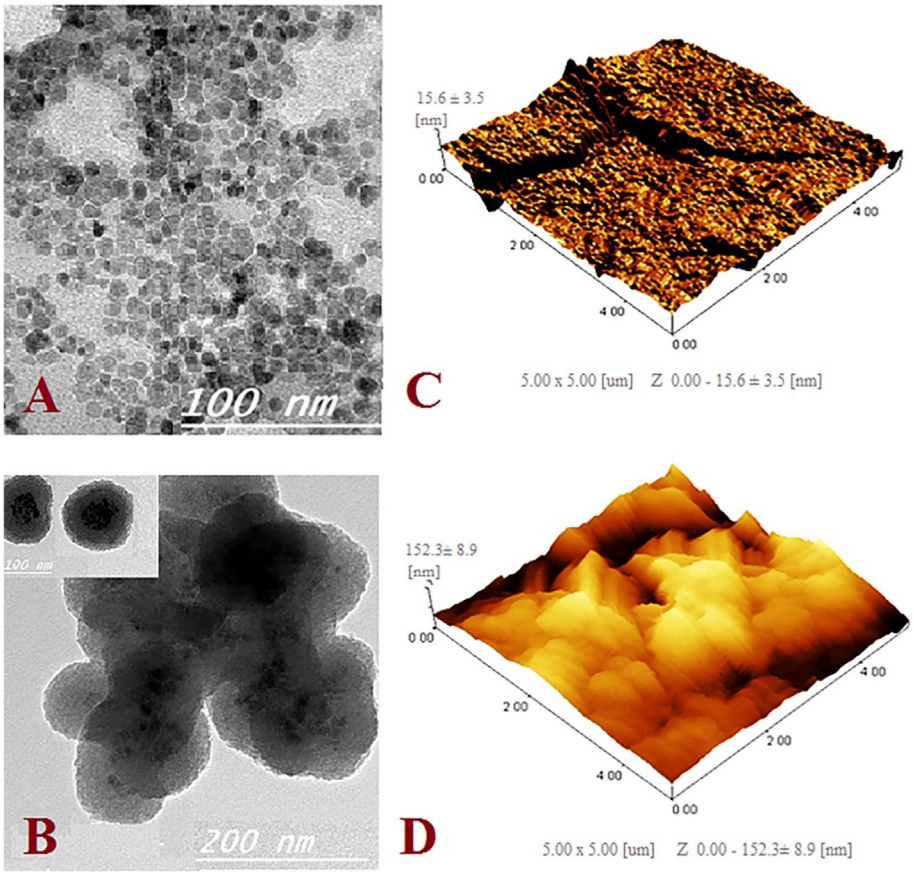

Fig. 2. (A) TEM image of IONPs, (B) TEM image of SIONPs,(C) AFM image of IONPs, (D) AFM image of SIONPs.

3.1.3. Surface charges

Zeta Potential/Particle Sizer detected surface charges of nanoparticles. For IONPs, the net negative surface charges were detected with an average value of -32 ± 1.8 mv due to the FeO^- group on the IONPs surface [41].

Silanol group (SiO^-) deprotonation on the surface of SIONPs led to a rise in the negative charge of its surface to -41 ± 2.3 mV, which means that the silica layer on the IONPs surface enhances its stability [42,43].

3.1.4. Magnetic study

At room temperature, the hysteresis loops of IONPs and SIONPs investigated using VSM are shown in Fig. 1B. IONPs and SIONPs exhibit an S-shape with no hysteresis loop curves. The retentivity (M_r) and the coercivity are close to zero, which indicates their superparamagnetic nature [44].

The saturation magnetization (M_s) values of IONPs and SIONPs witnessed a slight change from 0.57 emu/cm^3 in case IONPs to 0.39 emu/cm^3 in case SIONPs, which confirms that the silica layer did not negatively affect the magnetic properties of IONPs core.

Because of SIONPs' magnetic characteristics, it has great potential as an MRI contrast agent.

3.2. In vitro studies

3.2.1. Cell viability assay

Survival curves of MCF-7 cells incubated with different concentrations of IONPs and SIONPs and exposed to different doses of X-ray are represented in Fig. 3A–D.

ROS such as superoxide radicals ($O_2^{-\bullet}$), hydrogen peroxide (H_2O_2), and hydroxyl radicals ($OH^\bullet$) are produced inside the tumor cell treated with X-ray. This occurred through decomposing and ionizing water molecules associated with X-ray treatment leading to cellular damage and cell death [45]. The presence of high Z nanoparticles which absorb, and scatter X-ray enhances ROS production [46]. Photoelectrons, Compton and auger electrons, and fluorescence photons emitted in the cellular environment in these NPs lead to ionization and excitation of biological molecules with their migration [47]. Therefore, one of the major objectives of this work is to investigate the radioenhancing effect of IONPs and SIONPs.

Fig. 3A–D showed that, in the absence of nano-treatment, cells exposed to 0.5 and 1 Gy showed about 82% and 66.8%, respectively, while those exposed to 2 and 4 Gy showed the viability of about 46.3% and 44.3%, respectively.

When MCF-7 cells were incubated with different concentrations of IONPs 24h before irradiation, the effect of radiation damage increased compared to cells exposed to radiation only (Fig. 3A–D).

In comparison with cells exposed to radiation without nano-treatment, for 0.5 and 1 Gy, there were no significant decreases in the viability of cells treated with 5 and 10 μg/ml of IONPs. Nevertheless, cell viability significantly decreased with higher concentrations (20, 40, and 80 μg/ml).

DEF values of IONPs and SIONPs, which reflected the effect of IONPs and SIONPs as radiosensitizers, were tabulated in Table 2. Cells that were treated with 5 and 10 μg/ml of IONPs and irradiated with 1 Gy had DEF values of 1.13 and 1.11, respectively. Cells treated with 20, 40, and 80 μg/ml had DEF values of 1.25, 1.37, and 1.93, respectively. For 2 and 4 Gy doses, the viability of cells treated with IONPs showed a non-significant reduction due to the highly potent

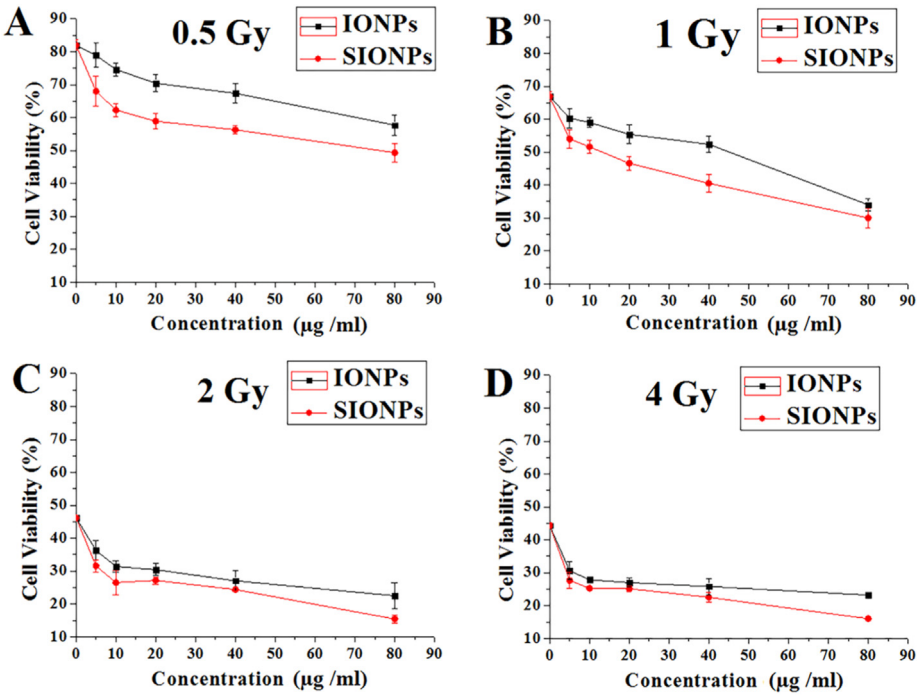

Fig. 3. Survival curves (A–D) of MCF-7 cells treated with different concentrations (0,5, 10, 20, 40 and 80 μg/ml, respectively) of IONPs and SIONPs and exposed to different radiation doses (0.5, 1, 2 and 4 Gy).

Table 2
Dose enhancement factor (DEF) values from the MTT assay for the MCF-7 cell line. The cells incubated with IONPs and SIONPs (5,10, 20, 40, 80 μg/ml concentrations) and irradiated with 6 MeV X-ray photon beam (0.5, 1, 2, 4 Gy).

Dose (Gy)	Dose Enhancement Factor (DEF)									
	Concentration (μg/ml)									
	IONPs					SIONPs				
	5	10	20	40	80	5	10	20	40	80
0.5	**1.00**	**1.09**	**1.16**	**1.25**	**1.42**	**1.21**	**1.32**	**1.39**	**1.46**	**1.66**
1	**1.13**	**1.11**	**1.25**	**1.37**	**1.93**	**1.24**	**1.30**	**1.43**	**1.65**	**2.20**
2	**1.27**	**1.47**	**1.52**	**1.71**	**2.06**	**1.47**	**1.74**	**1.72**	**1.89**	**3.00**
4	**1.50**	**1.65**	**1.70**	**1.72**	**1.91**	**1.46**	**1.75**	**1.69**	**1.96**	**2.76**

effect of radiation at high doses. The outcomes of the MTT reveal that IONPs increase the potency of X-ray beam against MCF-7 cells; it also demonstrates that the radio-enhancing effect of IONPs is concentration-dependent. The reduction of cell viability with the concentration may be due to the enhancement of cellular internalization, which leads to increased ROS production [48,49].

After coating IONPs with silica, the data confirmed that, at low doses of SIONPs treatment, there was an enhancement in the radiosensitizing effect over IONPs. With 0.5 Gy dose, DEF values of cells treated with 5 and 10 μg/ml of IONPs were 1 and 1.09, respectively, and those treated with SIONPs at these concentrations had DEF of 1.21 and 1.32, respectively.

This radiosensitization enhancement extended to higher concentrations of SIONPs (20, 40, and 80 μg/ml), DEF values of cells treated with these concentrations and irradiated with 1 Gy were 1.43, 1.65, and 2.2, respectively. Generally, the DEF of SIONPs, calculated for each concentration and dose, was higher than that of IONPs.

MTT results show that the optimum concentration of SIONPs was 80 μg/ml.

Interestingly, results show more powerful radiosensitization effects of SIONPs against MCF-7 cells than IONPs. This can be attributed to SIONPs surface roughness which increases the entrance of SIONPs through the cell membrane. This led to increased ROS generation in cells treated with SIONPs combined with radiation compared to those treated with IONPs with the same dose. SIONPs' surface roughness is approximately 1.3 times greater than those of IONPs, leading to enhanced SIONPs' cellular internalization compared with IONPs [27,36].

3.2.2. Comet assay

Interactions between ROS and biological molecules can contribute to breaks in single-strand or double-strand DNA and DNA–DNA or DNA–protein cross-linking, leading to cell death [50].

DNA damages in cells treated with an X-ray beam combined with the prepared nanoparticles can be represented by performing the comet assay. DNA damage has been studied to illustrate the radioenhancing effects of IONPs and SIONPs on MCF-7 cells. The DNA damages were expressed as Tail Length, % DNA tail, and tail moment (Fig. 4A, B).

The comet parameters of 0.5G3 and 1G3 and 0.5G4 and 1G4 showed non-significant differences. Compared with other groups, the comet parameters of 0.5G5 and 1G5 showed highly significant differences (Fig. 4A, B).

DNA damage rises with the radiation dose, and so it can be considered dose-dependent damage.

In contrast to other groups, a more serious significant DNA damage is shown in groups of cells incubated with 40 μg/ml SIONPs and irradiated with 0.5 Gy and 1Gy. This suggests a greater number of double-strand ruptures due to high ROS production [51].

MCF-7 cells incubated with 10 μg/ml SIONPs, 24hr before irradiation, demonstrated greater DNA damage with different doses as opposed to cells incubated with 10 μg/ml IONPs, 24hr before irradiation, suggesting increased internalization of SIONPs through cells and ROS generation in comparison with IONPs.

The results of cells incubated with 10 μg/ml SIONPs, 24hr before

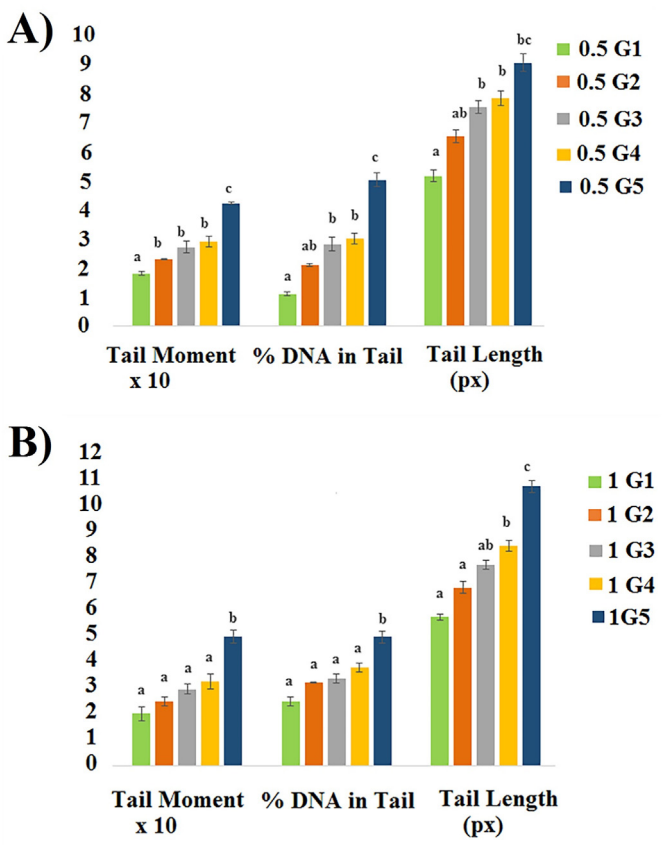

Fig. 4. DNA damage of MCF7 cells assessed by the Comet assay for 0.5G1 (control, untreated group) and treated groups: 0.5G2 (10 μg/ml of IO-MNPs), 0.5G3 (10 μg/ml of SIO-MNPs), 0.5G4 (40 μg/ml of IO-MNPs) and 0.5G5 (40 μg/ml of SIO-MNPs). All groups were exposed to an X ray photon beam at dose of: (A) 0.5 Gy, (B) 1 Gy. Different characters indicate significant ($p < 0.05$) different means.

irradiation, are extremely close to those of cells incubated with 40 μg/ml IONPs. This means that modest amounts of SIONPs can produce the same ROS proportion as high concentrations of IONPs. This might be related to SIONPs' improvement of cellular internalization and increased ROS production in cells compared to IONPs.

This study is an extension of a previous study that emphasized many advantages of SIONPs as multifunctional nanoparticles and explained the prospect of using them as a theragnostic agent in cancer therapy.

4. Conclusion

IONPs and SIONPs were successfully prepared using the co-precipitation protocol. The silica layer improved the stability of the nanocomposite without altering the magnetic behavior of the core IONPs. Therefore, SIONPs can be used as MRI contrast agents. When MCF 7 cells treated with an X-ray beam were combined with SIONPs, ROS generation increased compared to the combination of X-ray with IONPs. The results of the present study have shown that SIONPs had an extremely significant impact as radiosensitizing agents. This was emphasized in the low doses that, when combined with SIONPs, displayed the same powerful impact as the high radiation doses without using nanoparticles. During the treatment procedure, this will have a benefit in reducing the radiation dosage to healthy tissues.

Ethics approval and consent to participate

Not applicable.

Consent for publication

Not applicable.

Data availability

All data needed to support the conclusions are included in this article. Additional data related to this paper can be requested from the author (oashraf@sci.cu.edu.eg).

Authors' contributions

M.M.F. and H.M.F. designed this study, and O.A. wrote the main manuscript, performed the experiments, and prepared Figs. All authors reviewed the manuscript. All authors read and approved the final manuscript.

Funding

This work receives no funding

Declaration of competing interest

The authors declare that they have no competing interests.

Acknowledgments

Not applicable.

References

[1] R. Atun, D.A. Jaffray, M.B. Barton, F. Bray, M. Baumann, B. Vikram, T.P. Hanna, F.M. Knaul, Y. Lievens, T.Y.M. Lui, Expanding global access to radiotherapy, Lancet Oncol. 16 (2015) 1153–1186.
[2] K.D. Miller, R.L. Siegel, C.C. Lin, A.B. Mariotto, J.L. Kramer, J.H. Rowland, K.D. Stein, R. Alteri, A. Jemal, Cancer treatment and survivorship statistics, 2016, CA, Cancer J. Clin. 66 (2016) 271–289.
[3] S. Khoei, S.R. Mahdavi, H. Fakhimikabir, A. Shakeri-Zadeh, A. Hashemian, The role of iron oxide nanoparticles in the radiosensitization of human prostate carcinoma cell line DU145 at megavoltage radiation energies, Int. J. Radiat. Biol. 90 (2014) 351–356.
[4] A. Malik, M. Sultana, A. Qazi, M.H. Qazi, G. Parveen, S. Waquar, A.B. Ashraf, M. Rasool, Role of natural radiosensitizers and cancer cell radioresistance: an update, Anal. Cell Pathol. 2016 (2016).
[5] M. Krause, A. Dubrovska, A. Linge, M. Baumann, Cancer stem cells: radioresistance, prediction of radiotherapy outcome and specific targets for combined treatments, Adv. Drug Deliv. Rev. 109 (2017) 63–73.
[6] R. V Lalla, N. Treister, T. Sollecito, B. Schmidt, L.L. Patton, K. Mohammadi, J.S. Hodges, M.T. Brennan, O.S. Group, Oral complications at 6 months after radiation therapy for head and neck cancer, Oral Dis. 23 (2017) 1134–1143.
[7] F. Gao, D. Wang, T. Zhang, A. Ghosal, Z. Guo, Y. Miao, G. Li, X. Liu, J. Lu, J. Yu, Facile synthesis of Bi2S3-MoS2 heterogeneous nanoagent as dual functional radiosensitizer for triple negative breast cancer theranostics, Chem. Eng. J. (2020), 125032.
[8] H. Wang, X. Mu, H. He, X.-D. Zhang, Cancer radiosensitizers, Trends Pharmacol. Sci. 39 (2018) 24–48.
[9] S. Rey, L. Schito, M. Koritzinsky, B.G. Wouters, Molecular targeting of hypoxia in radiotherapy, Adv. Drug Deliv. Rev. 109 (2017) 45–62.
[10] Z. Xiong, J.-X. Zhong, Z. Zhao, T. Chen, Biocompatible ruthenium polypyridyl complexes as efficient radiosensitizers, Dalton Trans. 48 (2019) 4114–4118.
[11] V. Wagner, A. Dullaart, A.-K. Bock, A. Zweck, The emerging nanomedicine landscape, Nat. Biotechnol. 24 (2006) 1211.
[12] Y. Weng, J. Liu, S. Jin, W. Guo, X. Liang, Z. Hu, Nanotechnology-based strategies for treatment of ocular disease, Acta Pharm. Sin. B. 7 (2017) 281–291.
[13] D. V Alexandrov, N. Korabel, F. Currell, S. Fedotov, Dynamics of intracellular clusters of nanoparticles, Cancer Nanotechnol. 13 (2022) 1–13.
[14] A. Meidanchi, A. Motamed, Preparation, characterization and in vitro evaluation of magnesium ferrite superparamagnetic nanoparticles as a novel radiosensitizer of breast cancer cells, Ceram. Int. 46 (11) (2020) 17577–17583.
[15] M. Rezaei, K. Khoshgard, L. Hosseinzadeh, A. Haghparast, M.-T. Eivazi,

Application of Dextran-Coated Iron Oxide Nanoparticles in Enhancing the Radiosensitivity of Cancerous Cells in Radiotherapy with High-Energy Electron Beams, 2019.
[16] H. Fakhimikabir, M.B. Tavakoli, A. Zarrabi, A. Amouheidari, S. Rahgozar, The role of folic acid-conjugated polyglycerol coated iron oxide nanoparticles on radiosensitivity with clinical electron beam (6 MeV) on human cervical carcinoma cell line: in vitro study, J. Photochem. Photobiol. B Biol. 182 (2018) 71–76.
[17] S. Laurent, M. Mahmoudi, Superparamagnetic iron oxide nanoparticles: promises for diagnosis and treatment of cancer, Int. J. Mol. Epidemiol. Genet. 2 (2011) 367–390.
[18] J.S. Kim, T.-J. Yoon, K.N. Yu, B.G. Kim, S.J. Park, H.W. Kim, K.H. Lee, S.B. Park, J.-K. Lee, M.H. Cho, Toxicity and tissue distribution of magnetic nanoparticles in mice, Toxicol. Sci. 89 (2005) 338–347.
[19] A.S. Lübbe, C. Alexiou, C. Bergemann, Clinical applications of magnetic drug targeting, J. Surg. Res. 95 (2001) 200–206.
[20] A. Lu, E. emsp14L Salabas, F. Schüth, Magnetic nanoparticles: synthesis, protection, functionalization, and application, Angew. Chem. Int. Ed. 46 (2007) 1222–1244.
[21] O. Veiseh, C. Sun, J. Gunn, N. Kohler, P. Gabikian, D. Lee, N. Bhattarai, R. Ellenbogen, R. Sze, A. Hallahan, Optical and MRI multifunctional nanoprobe for targeting gliomas, Nano Lett. 5 (2005) 1003–1008.
[22] W. Wu, Q. He, C. Jiang, Magnetic iron oxide nanoparticles: synthesis and surface functionalization strategies, Nanoscale Res. Lett. 3 (2008) 397.
[23] F. Hu, K.G. Neoh, L. Cen, E.-T. Kang, Cellular response to magnetic nanoparticles “PEGylated” via surface-initiated atom transfer radical polymerization, Biomacromolecules 7 (2006) 809–816.
[24] Z. Zhang, L. Zhang, L. Chen, L. Chen, Q. Wan, Synthesis of novel porous magnetic silica microspheres as adsorbents for isolation of genomic DNA, Biotechnol. Prog. 22 (2006) 514–518.
[25] Z. Lu, J. Dai, X. Song, G. Wang, W. Yang, Facile synthesis of Fe3O4/SiO2 composite nanoparticles from primary silica particles, Colloids Surfaces A Physicochem. Eng. Asp. 317 (2008) 450–456.
[26] M. Shahriary, H. Veisi, M. Hekmati, S. Hemmati, In situ green synthesis of Ag nanoparticles on herbal tea extract (Stachys lavandulifolia)-modified magnetic iron oxide nanoparticles as antibacterial agent and their 4-nitrophenol catalytic reduction activity, Mater. Sci. Eng. C. 90 (2018) 57–66.
[27] M.M. Fathy, H.M. Fahmy, O.A. Saad, W.M. Elshemey, Silica-coated iron oxide nanoparticles as a novel nano-radiosensitizer for electron therapy, Life Sci. 234 (2019), 116756, https://doi.org/10.1016/j.lfs.2019.116756.
[28] E. Catalano, M. Miola, S. Ferraris, S. Novak, F. Oltolina, A. Cochis, M. Prat, E. Vernè, L. Rimondini, A. Follenzi, Magnetite and silica-coated magnetite nanoparticles are highly biocompatible on endothelial cells in vitro, Biomed, Phys. Eng. Express. 3 (2017), 25015.
[29] S. Klein, M.L. Dell'Arciprete, M. Wegmann, L.V.R. Distel, W. Neuhuber, M.C. Gonzalez, C. Kryschi, Oxidized silicon nanoparticles for radiosensitization of cancer and tissue cells, Biochem. Biophys. Res. Commun. 434 (2013) 217–222.
[30] N.S. Elbialy, M.M. Fathy, W.M. Khalil, Preparation and characterization of magnetic gold nanoparticles to be used as doxorubicin nanocarriers, Phys. Med. 30 (2014) 843–848.
[31] A. Monks, D. Scudiero, P. Skehan, R. Shoemaker, K. Paull, D. Vistica, C. Hose, J. Langley, P. Cronise, A. Vaigro-Wolff, Feasibility of a high-flux anticancer drug screen using a diverse panel of cultured human tumor cell lines, JNCI J. Natl. Cancer Inst. 83 (1991) 757–766.
[32] I. Sondi, B. Salopek-Sondi, Silver nanoparticles as antimicrobial agent: a case study on E. coli as a model for Gram-negative bacteria, J. Colloid Interface Sci. 275 (2004) 177–182.
[33] R.C. Murdock, L. Braydich-Stolle, A.M. Schrand, J.J. Schlager, S.M. Hussain, Characterization of nanomaterial dispersion in solution prior to in vitro exposure using dynamic light scattering technique, Toxicol. Sci. 101 (2008) 239–253.
[34] K. Takahashi, H. Kato, T. Saito, S. Matsuyama, S. Kinugasa, Precise measurement of the size of nanoparticles by dynamic light scattering with uncertainty analysis, Part. Part. Syst. Char. 25 (2008) 31–38.
[35] W. Libo, J. Zhang, W. Watanabe, Physical and chemical stability of drug nanoparticles, Adv. Drug Deliv. Rev. 63 (2011) 456–469.
[36] Y. Yin, Y. Lu, Y. Sun, Y. Xia, Silver nanowires can be directly coated with amorphous silica to generate well-controlled coaxial nanocables of silver/silica, Nano Lett. 2 (2002) 427–430.
[37] Y.-S. Lin, C.L. Haynes, Impacts of mesoporous silica nanoparticle size, pore ordering, and pore integrity on hemolytic activity, J. Am. Chem. Soc. 132 (2010) 4834–4842.
[38] C. LoPresti, M. Massignani, C. Fernyhough, A. Blanazs, A.J. Ryan, J. Madsen, N.J. Warren, S.P. Armes, A.L. Lewis, S. Chirasatitsin, Controlling polymersome surface topology at the nanoscale by membrane confined polymer/polymer phase separation, ACS Nano 5 (2011) 1775–1784.
[39] Y. Niu, M. Yu, S.B. Hartono, J. Yang, H. Xu, H. Zhang, J. Zhang, J. Zou, A. Dexter, W. Gu, Nanoparticles mimicking viral surface topography for enhanced cellular delivery, Adv. Mater. 25 (2013) 6233–6237.
[40] K. Rechendorff, M.B. Hovgaard, M. Foss, V.P. Zhdanov, F. Besenbacher, Enhancement of protein adsorption induced by surface roughness, Langmuir 22 (2006) 10885–10888.
[41] A.L. Andrade, D.M. Souza, M.C. Pereira, J.D. Fabris, R.Z. Domingues, Synthesis and characterization of magnetic nanoparticles coated with silica through a sol-gel approach, Cerâmica 55 (2009) 420–424.
[42] A.A. Christy, P.K. Egeberg, Quantitative determination of surface silanol groups in silicagel by deuterium exchange combined with infrared spectroscopy and chemometrics, Analyst 130 (2005) 738–744.
[43] A.H.F. Lee, S.F. Gessert, Y. Chen, N. V Sergeev, B. Haghiri, Preparation of iron oxide silica particles for Zika viral RNA extraction, Heliyon 4 (2018), e00572.
[44] Z. Li, M. Kawashita, N. Araki, M. Mistumori, M. Hiraoka, Effect of particle size of magnetite nanoparticles on heat generating ability under alternating magnetic field, Bioceram. Dev. Appl. 1 (2011).
[45] S. Her, D.A. Jaffray, C. Allen, Gold nanoparticles for applications in cancer radiotherapy: mechanisms and recent advancements, Adv. Drug Deliv. Rev. 109 (2017) 84–101.
[46] A. Mesbahi, A review on gold nanoparticles radiosensitization effect in radiation therapy of cancer, Rep. Practical Oncol. Radiother. 15 (2010) 176–180.
[47] D. Kwatra, A. Venugopal, S. Anant, Nanoparticles in radiation therapy: a summary of various approaches to enhance radiosensitization in cancer, Transl. Cancer Res. 2 (2013) 330–342.
[48] K. Khoshgard, P. Kiani, A. Haghparast, L. Hosseinzadeh, M.T. Eivazi, Radiation dose rate affects the radiosensitization of MCF-7 and HeLa cell lines to X-rays induced by dextran-coated iron oxide nanoparticles, Int. J. Radiat. Biol. 93 (2017) 757–763.
[49] M. Zabihzadeh, S.S. Arefian, N. Shams, Dose Enhancement Due to Injection of 79Au, 64Ga, 26Fe and 22Ti Nanoparticles into Tumor during HDR-192Ir Brachytherapy Treatment: Monte Carlo Study, 2013.
[50] D.M. Sridharan, A. Asaithamby, S.M. Bailey, S.V. Costes, P.W. Doetsch, W.S. Dynan, A. Kronenberg, K.N. Rithidech, J. Saha, A.M. Snijders, E. Werner, C. Wiese, F.A. Cucinotta, J.M. Pluth, Understanding cancer development processes after HZE-particle exposure: roles of ROS, DNA damage repair and inflammation, Radiat. Res. 183 (2015) 1–26, https://doi.org/10.1667/RR13804.1.
[51] S. Havaki, A. Kotsinas, E. Chronopoulos, D. Kletsas, A. Georgakilas, V.G. Gorgoulis, The role of oxidative DNA damage in radiation induced bystander effect, Cancer Lett. 356 (2015) 43–51.